PERGAMON

International Journal of Heat and Mass Transfer 44 (2001) 605–618

International Journal of HEAT and MASS TRANSFER

www.elsevier.com/locate/ijhmt

Parametric study of metal droplet deposition and solidification process including contact resistance and undercooling effects

Mo Chung [1], R.H. Rangel*

Department of Mechanical and Aerospace Engineering, University of California, Irvine, CA 92697-3975, USA

Received 4 June 1999; received in revised form 15 March 2000

Abstract

The effects of process parameters on metal droplet spreading and solidification are investigated numerically. The parameters include the impinging velocity, contact resistance between the droplet and substrate, and degree of undercooling associated with rapid phase change. A simplified model is adopted to describe the splat size evolution and energy equations for the liquid, solidified layer, and substrate are simultaneously solved to analyze heat transfer processes during solidification. The energy equations are coupled by boundary conditions such as contact resistance and undercooling in a regularized calculation domain formed by means of algebraic grid generation. The results reveal that impinging velocity and contact resistance have strong effects on both final splat size and solidification time. The effects of undercooling are not significant unless the nucleation temperature is low in relation to the initial liquid superheating.

1. Introduction

Research in materials processing has recently focused on the development of novel processing methodologies for the production of high quality surface properties. Spray and droplet-based manufacturing are good examples of such methodologies that can produce protective films on substrates. Scientific and engineering issues involving droplet deposition and heat transfer have drawn a great deal of attention among researchers due to its wide range of industrial applications. Various theoretical studies have been conducted to investigate droplet based deposition processes. El-Kaddah et al. [1] derived a one-dimensional analytical solution to a thermal spray process based on the Stefan model and extended it to two-dimensions by means of numerical solution. Madejski [2] proposed a splat deformation and solidification model assuming that the liquid portion of the splat is shaped as a cylinder. From a conservation of mechanical energy principle, he derived a relation for the growth of the radius of the disk while using the Neumann solution to the one-dimensional Stefan solidification problem in conjunction with an integral approach. An improvement over Madjeski's model has been presented by Delplanque and Rangel [3] utilizing the more appropriate velocity profile suggested by

* Corresponding author. Tel.: +1-949-824-4033; fax: +1-949-824-8585.

E-mail address: rhrangel@uci.edu (R.H. Rangel).

[1] On Leave from Department of Mechanical Engineering, Yeungnam University, 214-1 Dae-dong, Kyungsan, Korea 712-749

0017-9310/01/$ - see front matter
PII: S0017-9310(00)00112-5

Nomenclature

b	liquid thickness
Bi	Biot number
D	droplet diameter
E_k	kinetic energy
E_p	potential energy
E_Φ	energy dissipation
Ec	$V^2/C_{pl}(T_m - T_{u0})$, Eckert number
h_i	contact heat transfer coefficient
$h_{c,u}$	convective heat transfer coefficient for substrate upper surface
h_{sf}	latent heat of solidification
h_{side}	convective heat transfer coefficient for splat side surface
h_{top}	convective heat transfer coefficient for splat upper surface
k	thermal conductivity of solid
k_{sl}	ratio of the solid to liquid-phase thermal conductivity, k_s/k_l
k_{ul}	ratio of the substrate to liquid thermal conductivity, k_u/k_l
K_m	kinetics coefficient for undercooling solidification
Pe	$Re\,Pr = VD/\alpha_l$, Peclet number for liquid droplet
Pr	ν_l/α, liquid droplet Prandtl number
Re	VD/ν_l, Reynolds number for liquid droplet
R	droplet radius
s	solid front position
Ste	$C_{pl}(T_{l0} - T_m)/h_{sf}$, Stefan number
t	time
T_a	ambient fluid temperature
T_{lo}	liquid droplet initial temperature
T_m	equilibrium melting temperature
T_{nucle}	nucleation temperature
T_{uo}	substrate initial temperature
ΔT	$T_m - T_{uo}$, reference temperature difference
ΔT_{nucle}	$T_m - T_{nucle}$, undercooling
V	droplet impinging velocity
We	$\rho D V^2/\sigma$, Weber number for liquid droplet

Greek symbols

α	thermal diffusivity
α_{sl}	ratio of the solid- to liquid-phase thermal conductivity, α_s/α_l
α_{ul}	ratio of the substrate to liquid thermal diffusivity, α_u/α_l
$\tilde{\Phi}$	$\Phi D^2/V^2$, nondimensional dissipation function
μ	liquid droplet dynamic viscosity
ν	liquid droplet kinematic viscosity
θ	normalized temperature, $(T - T_{u0})/\Delta T$
$\Delta\theta_n$	$(T_m - T_{nucle})/\Delta T$, dimensionless undercooling
ρ	density of liquid
σ	surface tension coefficient
τ	dimensionless time

Subscripts

i	substrate–splat interface
l	liquid droplet
m	melting
o	initial
s	solidified layer
sf	solid front
u	substrate

Superscript

$*$	nondimensional

Markworth and Sanders [4] and an accurate derivation of the viscous energy dissipation. Numerical studies of droplet deposition processes based on the solution of the Stefan problem were contributed by Liu et al. [5], San Marchi et al. [6], Watanabe et al. [7] and Amon and Schmaltz. [8]. One of the problems associated with the application of the Stefan solution is that it does not account for the fluid motion and the effect of finite liquid thickness [8,9]. The effect of liquid motion on the solidification behaviour during the deposition process has been studied by Rangel and Bian [10,11] through the study of the stagnation flow solidification problem. More recently, they addressed the case of substrate remelting [12] with a model based on the solution of the mechanical energy equation combined with the solution of the transient thermal energy equation in both the solid and liquid phases. Aside from these idealized models, numerical solution of the incompressible Navier–Stokes equations has also been carried out either by finite element or finite difference method [13–15] with varying degree of sophistication.

Two important issues in modeling droplet deformation and solidification are contact resistance and undercooling. The quality of thermal contact between the substrate and splat plays an important role in the process. Wang and Matthys [16,17] investigated the contact resistance effects experimentally and numerically. Large scales of undercooling may exist in nonequilibrium conditions incurred by the rapid solidification at the interface. Under these

conditions, the phase change interface is not in thermodynamic equilibrium and the interface velocity is affected by the kinetic effects in addition to the heat removal rate [18]. Wang and Matthys [16,17] and Kang et al. [19] studied the mechanism of undercooling during rapid solidification by proposing a simple model.

In this study, we investigate the mechanisms controlling droplet spreading with an approximate model. This numerical tool can analyze the effects of parameters such as contact resistance, undercooling in addition to process and environmental parameters. The existence of contact resistance affects the solidification process significantly. In the idealized models without contact resistance and undercooling, the liquid–substrate interface temperature reaches the melting temperature specified by the thermodynamic equilibrium at the moment of impact, and solidification (or remelting of the substrate) starts immediately. When contact resistance exists, the droplet and substrate temperatures at the contact surface approach each other until either side reaches the phase change temperature. The temperature variations on both sides depend on the initial temperatures, properties of both materials, and magnitude of the contact resistance. The substrate is in contact with the liquid in the early stages of the spreading process. Later, the substrate is in contact with the solidified layer of the splat after a short transition period when the substrate is in contact with either liquid or solid phases depending on the location along the phase change interface. The mechanism of crystal growth kinetics for undercooling solidification is included to replace the classical assumption of thermodynamic equilibrium at the phase change interface to account for rapid solidification effects.

2. Theoretical considerations

Fig. 1 shows the physical model for the splat deformation and solidification process adopted in this study. A liquid droplet of diameter D impinges on a cold substrate with velocity V. The splat assumes a cylindrical shape (Madjeski model [2]) after the impact and as it spreads and solidifies on the substrate. While a full numerical simulation can handle the deformation of the free surface in a more realistic manner [5,13–15], it may hinder our ability to concentrate on one or two specific issues since many physical phenomena are simulated together. A model such as the one used here, which is geometrically simpler, permits us to investigate certain phenomena, in this case, contact resistance and undercooling in a more direct way.

We divide the process into three distinct stages in the presence of contact resistance. In the first stage of the process, the liquid–substrate interface temperature has not reached the phase change temperature and the liquid splat spreads without solidification. There are only two domains namely the liquid splat and the substrate and a contact resistance exists at the interface. Stage II is characterized by a thin, partly-formed solid layer over the substrate. The interface temperature is still above the phase change temperature at certain portions of the interface. Three distinct domains, namely the liquid, the solidified layer, and the substrate can be defined. Contact resistance exists at the substrate/solid layer or liquid–substrate interface

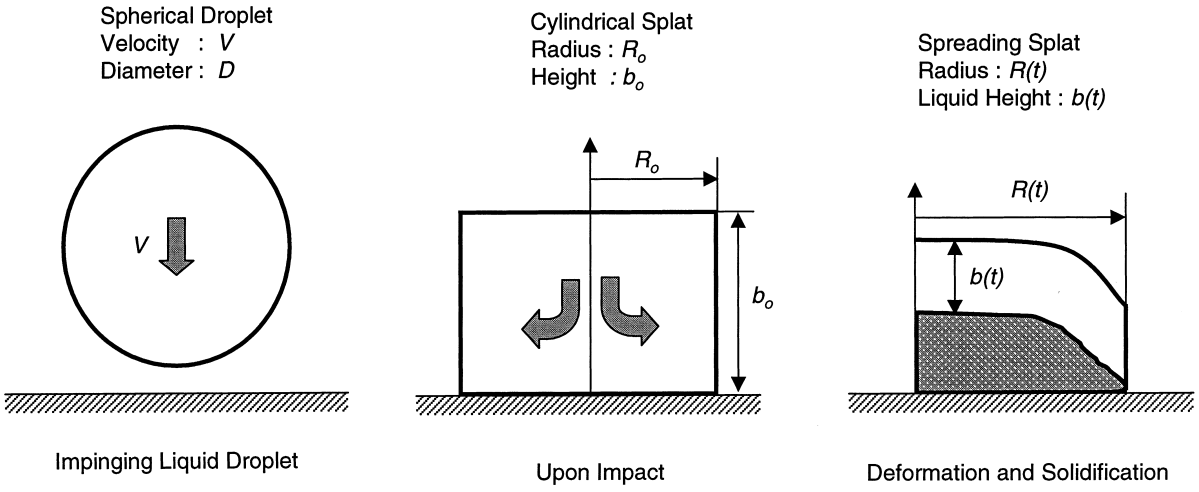

Fig. 1. An overview of the droplet spreading and solidification model.

Table 1
Governing equations and auxiliary conditions in physical domain

Item	Liquid	Solidified layer	Substrate
Governing equation	$\frac{\partial\theta}{\partial t^*}+u_r^*\frac{\partial\theta}{\partial r^*}+u_z^*\frac{\partial\theta}{\partial z^*}=\frac{1}{Pe}\left(\frac{1}{r^*}\frac{\partial\theta}{\partial r^*}+\frac{\partial^2\theta}{\partial r^{*2}}+\frac{\partial^2\theta}{\partial z^{*2}}\right)+\frac{Ec\tilde{\Phi}}{Re}$	$\frac{\partial\theta_s}{\partial t^*}=\frac{1}{Re'Pr_s}\left(\frac{1}{r^*}\frac{\partial\theta_s}{\partial r^*}+\frac{\partial^2\theta_s}{\partial r^{*2}}+\frac{\partial^2\theta_s}{\partial z^{*2}}\right)$	$\frac{\partial\theta_u}{\partial t^*}=\frac{1}{RePr_u}\left(\frac{1}{r^*}\frac{\partial\theta_u}{\partial r^*}+\frac{\partial^2\theta_u}{\partial r^{*2}}+\frac{\partial^2\theta_u}{\partial z^{*2}}\right)$
Initial condition	$\theta(r^*,z^*,0)=\theta_0=\frac{T_{l0}-T_m}{T_{u0}-T_m}$	$\theta_s\left(r^*,z^*,t_c^*\right)=\frac{T_{nucle}-T_m}{T_{u0}-T_m}$	$\theta_u(r^*,z^*,0)=0$
Top boundary condition	Convective heat loss $Bi_{top}[\theta-\theta_a]+\vec{n}\cdot\nabla\theta\|_{z^*=b^*}=0,\quad 0\le r^*\le R^*$	Undercooling model $\frac{\partial_s^*(t^*,r^*)}{\partial t^*}=-K_m^*\theta_s(r^*,s^*,t^*)$	$Bi_i\frac{k}{k_u}[\theta-\theta_u]+\frac{\partial\theta_u}{\partial z^*}=0,\quad 0\le r^*\le R^*$ $Bi_{c,\,u}(\theta_a-\theta_u)+\frac{\partial\theta_u}{\partial z^*}\Big\|_{z^*=0}=0,\quad R^*\le r^*\le\infty$
Bottom boundary condition	Contact resistance $Bi_i(\theta-\theta_u)-\frac{\partial\theta}{\partial z^*}\Big\|_{z^*=0}=0$	Contact resistance $Bi_i\frac{k}{k_s}(\theta_s-\theta_u)-\frac{1}{s^*}\frac{\partial\theta_s}{\partial z^*}\Big\|_{z^*=0}=0$	$\theta_u(r^*,-\infty,t^*)=0\quad 0\le r^*\le\infty$
Side boundary condition	Convective heat loss $Bi_{side}(\theta-\theta_u)-\frac{\partial\theta}{\partial r^*}\Big\|_{r^*=R^*}=0$	Wetting condition $\theta_s(R^*,0,t^*)=1$	$\theta_u(\infty,z^*,t^*)=0,\quad 0\le z^*\le\infty$
Center-line boundary condition	$\frac{\partial\theta}{\partial r^*}\Big\|_{r^*=0}=0\quad 0\le z^*\le b^*$	$\frac{\partial\theta_s}{\partial r^*}\Big\|_{r^*=0}=0\quad 0\le z^*\le b^*$	$\frac{\partial\theta_u}{\partial r^*}\Big\|_{r^*=0}=0\quad 0\le z^*\le 1$

depending on the location. From a computational point of view, this stage is the most difficult to model due to the complex morphology of the associated domains. In general, the shape and location of the solid layer on the substrate are not prescribed and should be found as a part of the solution. As Stage II progresses, the width of solidified layer increases until it covers the entire substrate. This event defines the starting point for Stage III. Three domains, namely liquid, solidified layer, and substrate are defined, while the liquid and solidified layer domains can be characterized by a common splat radius. There is a contact resistance at the substrate/solidified layer interface.

As in Madjeski's original model [2], the splat is assumed to be incompressible. At the beginning of the process ($t = 0$), the liquid droplet assumes the shape of a cylinder of radius R_0 and height b_0. The height of liquid layer of the droplet is assumed to be uniform across the radial direction meaning that the droplet outer contour is determined by the shape of solidified layer which can be determined by time integration of the local solidification rate. The thermophysical properties of the medium are constant but can be different in each phase except for density which is the same throughout. A contact resistance of uniform magnitude across the plane of contact of the splat and substrate is assumed along with an undercooling model that relates the phase change temperature with the thermodynamic equilibrium temperature.

Table 2
Paramater values for base case

Item	Value
D (m)	0.001
V (m/s)	10
T_m (K)	933
T_{uo} (K)	300
T_{lo} (K)	1033
T_a (K)	300
k_l (W/m K)	237
k_{sl}	0.4
k_{ul}	0.5
α_l (m^2/s)	3.63E−05
α_{sl}	0.43
α_{ul}	4
Pr_l	1.30E−02
Re	2.12E+04
We	266
Ste	1.67
Ec	9.20E−04
Bi_{sub}	0
Bi_{top}	0
Bi_{side}	0
Bi_i	10

2.1. Governing equations and auxiliary conditions

The governing equations in the physical domain are nondimensionalized using the droplet diameter D, droplet impact velocity V and the characteristic time D/V as the reference quantities. The reference temperature difference is $T_m - T_{uo}$.

2.1.1. Mechanical energy

The splat size evolution is governed by a mechanical energy conservation equation

$$\frac{d}{dt}(E_k + E_p) = -\frac{dE_\phi}{dt} \tag{1}$$

and an equation of conservation of mass to obtain the thickness of the liquid portion of the splat:

$$b(t) = \frac{D^3}{6R(t)^2} - \frac{m_s(t)}{\rho\pi R(t)^2} = \frac{D^3}{6R(t)^2} - s_{avg}(t) \tag{2}$$

Eqs. (1) and (2) are solved by using an integral approach coupled with the solution of the thermal energy equations described below. Details may be found in Ref. [20].

2.1.2. Thermal energy

Three separate domains namely the liquid splat, the solidified layer, and the substrate are defined for computational purpose. The energy equation for the solid layer and the substrate is the unsteady conduction equation. The energy equation for the liquid portion of the splat contains convective terms due to the spreading. Table 1 summarizes the governing equations and associated boundary conditions for each domain. The boundary conditions in the table include nondimensional forms of the following contact resistance equation

$$h_i \Delta T - k\frac{\partial T}{\partial z}\bigg|_{z=z_i} = 0 \tag{3}$$

and the linearized solid growth rate

$$\frac{\partial s}{\partial t} = K_m(T_m - T_{sf}) \tag{4}$$

In addition to the temperature boundary conditions at the phase change interface, the following nondimensional form of interface energy balance is used [21]

$$\frac{\partial s^*}{\partial t^*} = \frac{Ste}{Pe_l}\left[1 + \left(\frac{\partial s^*}{\partial r^*}\right)^2\right]\left[\frac{k_s}{k_l}\frac{\partial \theta_s}{\partial z^*}\bigg|_{z^*=z_i^*} - \frac{\partial \theta_l}{\partial z^*}\bigg|_{z^*=z_i^*}\right] \tag{5}$$

which is solved to yield metric information for the associated coordinate transformation.

The deforming physical domains of the liquid, solidi-

fied layer, and substrate can be mapped onto fixed rectangular domains by a number of coordinate transformations (algebraic grid generation). The energy equations for the three calculation domains can be casted into the following canonical form

$$\frac{\partial \vartheta}{\partial \tau} = A\frac{\partial \vartheta}{\partial \xi} + B\frac{\partial \vartheta}{\partial \eta} + C\frac{\partial^2 \vartheta}{\partial \xi^2} + D\frac{\partial^2 \vartheta}{\partial \eta^2} + E\frac{\partial^2 \vartheta}{\partial \xi \partial \eta} + F \quad (6)$$

where ϑ represents θ, θ_s, θ_u depending on the domain where the calculation is performed. Detailed information regarding the transformation and the numerical procedures for the solution of the governing equations can be found in Ref. [20].

3. Results and discussion

We present the effects of several parameters in reference to a base case. The parameter values for the base case are listed in Table 2. The base case corresponds to a 1 mm diameter aluminum droplet impinging on a cold iron substrate.

3.1. Effect of impinging velocity

As expected, the impinging velocity has a significant effect on the process. Figs. 2 and 3 compare the spreading and solidification behavior for two different values of the impinging velocity. These figures show the splat height and radius, liquid–solid interface location, and isotherms. Fig. 2 corresponds to the base case (10 m/s) while in the case of Fig. 3 the velocity is 1 m/s. As expected, the spreading is faster for the higher impinging velocity because the splat has more initial kinetic energy (100:1). The temperature distribution is also affected by the impinging velocity. The highest temperature in the splat occurs at the intersection of the upper splat surface with the axis of symmetry for the cases where adiabatic boundary

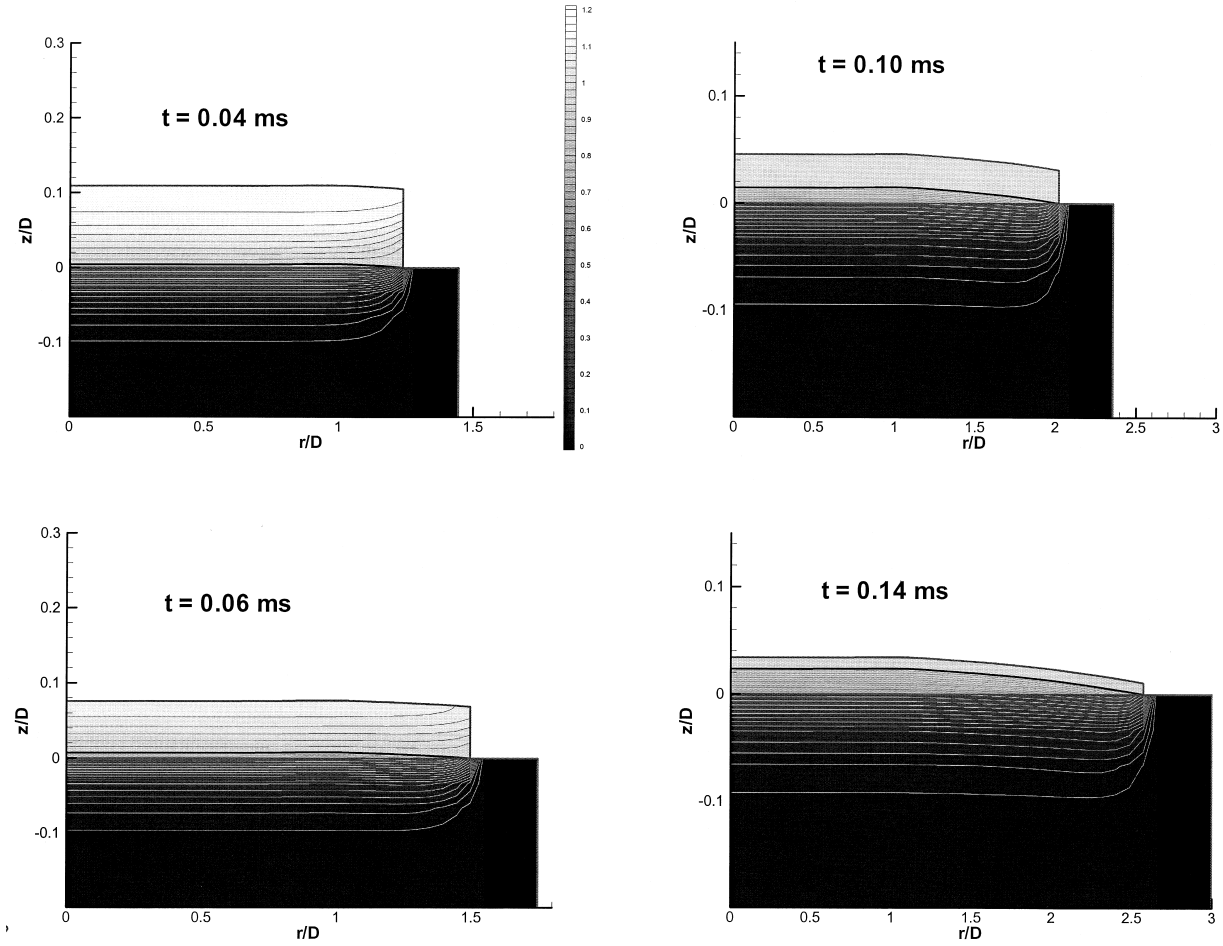

Fig. 2. Time evolution of splat deformation and solidification (case 1).

conditions are imposed on the upper splat surface. The isotherms in the splat and the substrate are nearly parallel to the interface but multidimensional effects are significant at the rim of the spreading splat where the highest temperature gradient in the substrate is observed.

Fig. 4 shows the time evolution of the splat radius, liquid thickness, and solid fraction for 10 and 1 m/s. A key difference between the high and low impinging velocities is observed in the behavior of the spreading rate R'. This is nearly constant for most of the spreading and solidification process but drops substantially near the completion of solidification for the higher velocity case. For the low velocity case, the spreading rate decreases during most of the process. Fig. 5 shows the solid front location, $s^*(r^*, t^*)$, in the splat at various instants of time cases 1 and 2. The morphology of the splat and interface location is significantly different depending on the impinging speed. In both cases, a bump in the solid front is noticeable near the rim of the splat. This is due to the fact that solidification invariably begins at the rim of the spreading splat where the heat transfer rate to the substrate is highest. The bump is more noticeable at higher impinging velocity but tends to smooth itself out over time. The early front general shape is nearly conserved to the completion of the solidification and it will eventually determine the final shape of the solidified splat. The solid layer first extends all the way across the splat at 0.014 and 0.023 ms for cases 1 and 2, respectively.

3.2. Effect of contact resistance

As it will be seen below, contact resistance predominantly affects the process time and final splat size. The existence of contact resistance gives rise to a finite temperature jump at the splat/substrate interface. This temperature jump reduces the magnitude of the tem-

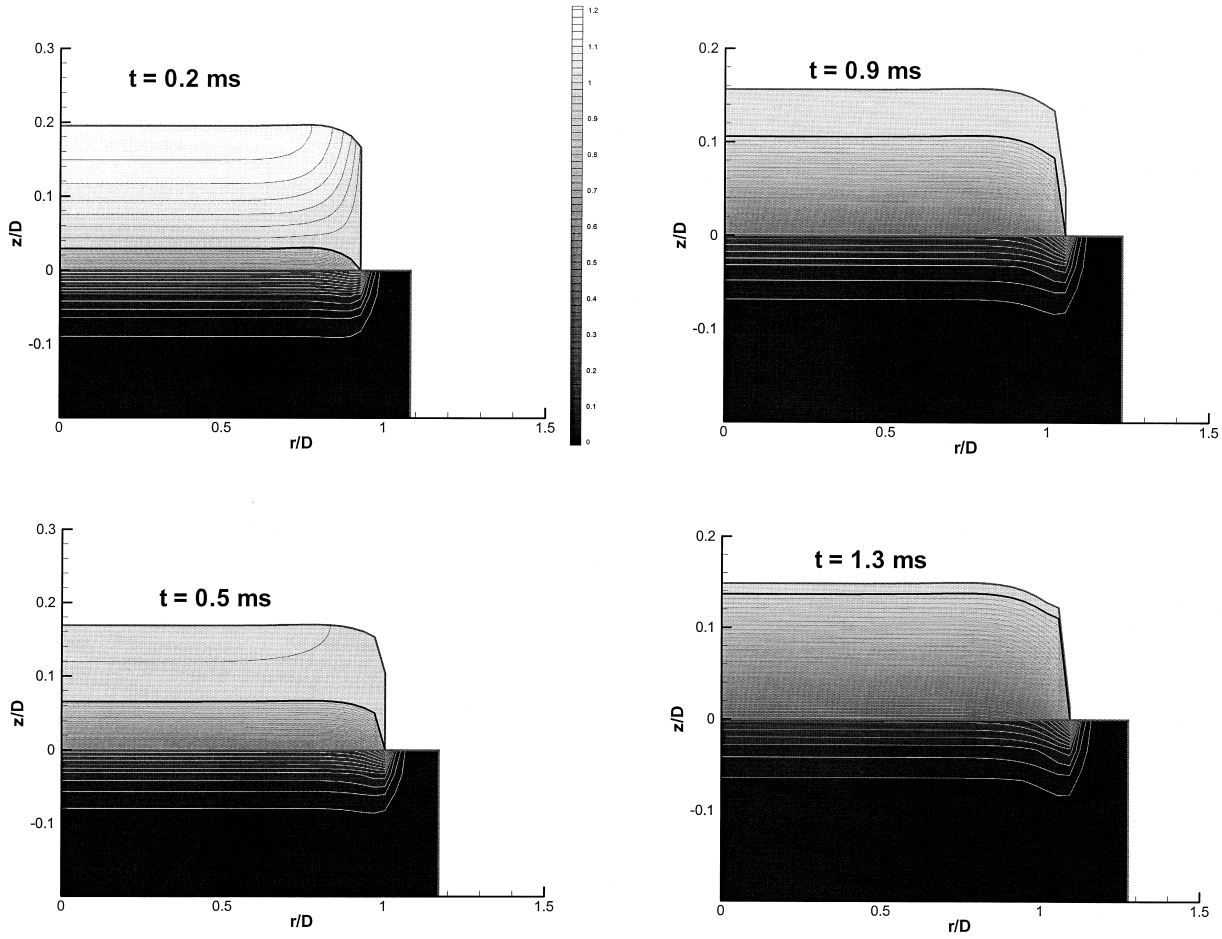

Fig. 3. Time evolution of splat deformation and solidification (case 2).

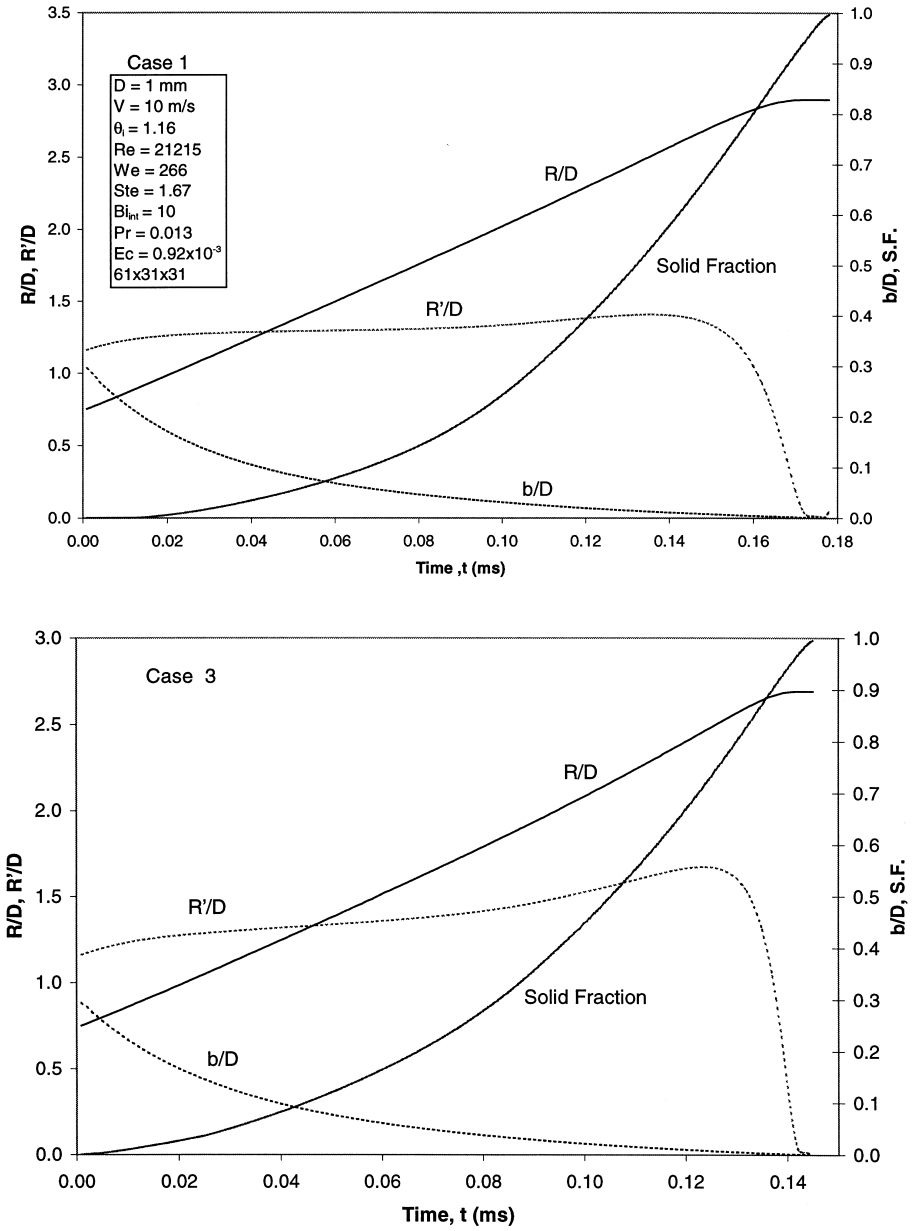

Fig. 4. Splat size and solid fraction evolution for high speed impingement (10 m/s).

perature gradients on both sides across this contact surface. Fig. 6 shows temperature distributions along the axis of the splat from within the substrate to the top of the splat for different instants of time and for the base case. At early times, for example at $t = 0.01$ ms, the splat temperature is above the melting point and the splat is fully liquid. At the contact surface, a temperature jump exists. At $t = 0.02$ ms, the splat temperature at the contact surface reaches the phase change value and solidification starts. A contact resistance remains between the solidified layer and the substrate. The temperature gradient in the liquid decreases as the process continues and the liquid temperature approaches a uniform value. The magnitude of the temperature jump decreases with time throughout the process but the jump persists even after the completion of solidification. In Fig. 6, the black dots indicate the position of the upper splat surface. Vertical tempera-

ture profiles at other radial locations have similar characteristics to those along the vertical axis.

The effect of contact resistance can be assessed in terms of process time and final splat radius. Fig. 7 shows the splat radius and solid fraction evolution for different values of the contact Biot number (the contact resistance is inversely proportional to the contact Biot number). The process time increases as contact resistance increases. Contact resistance delays the onset of solidification at the contact surface as explained in reference to Fig. 6. The process time and final splat size is strongly influenced by this delay. Fig. 8 shows the nucleation and complete solidification times (a) and the splat size at nucleation and at complete solidification (b) as functions of the contact Biot number. These four variables asymptotically approach their limits for the case without contact resistance as the contact Biot number (the nondimensional contact conductance) becomes large. The final splat radius can be substantially increased with high contact resistance.

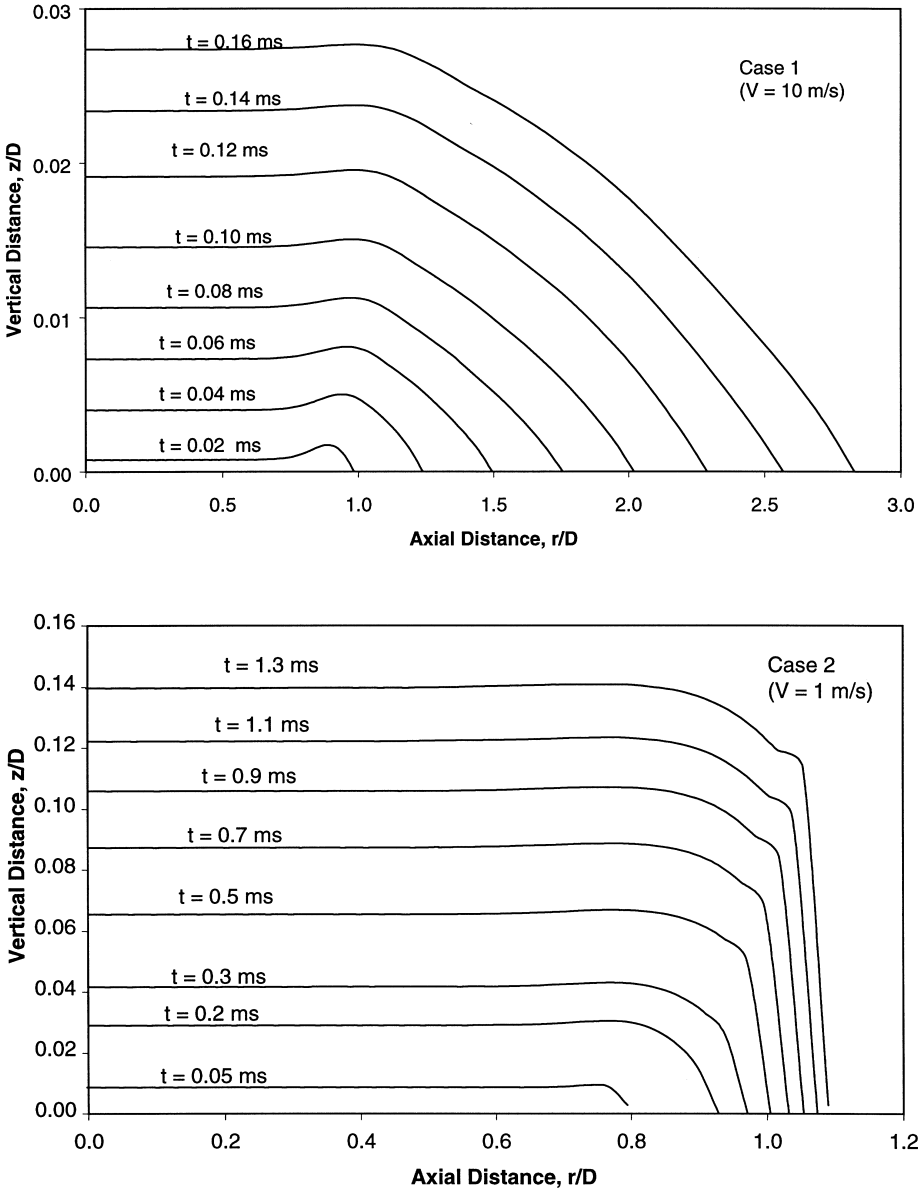

Fig. 5. Interface location evolution. (a) case 1, (b) case 2.

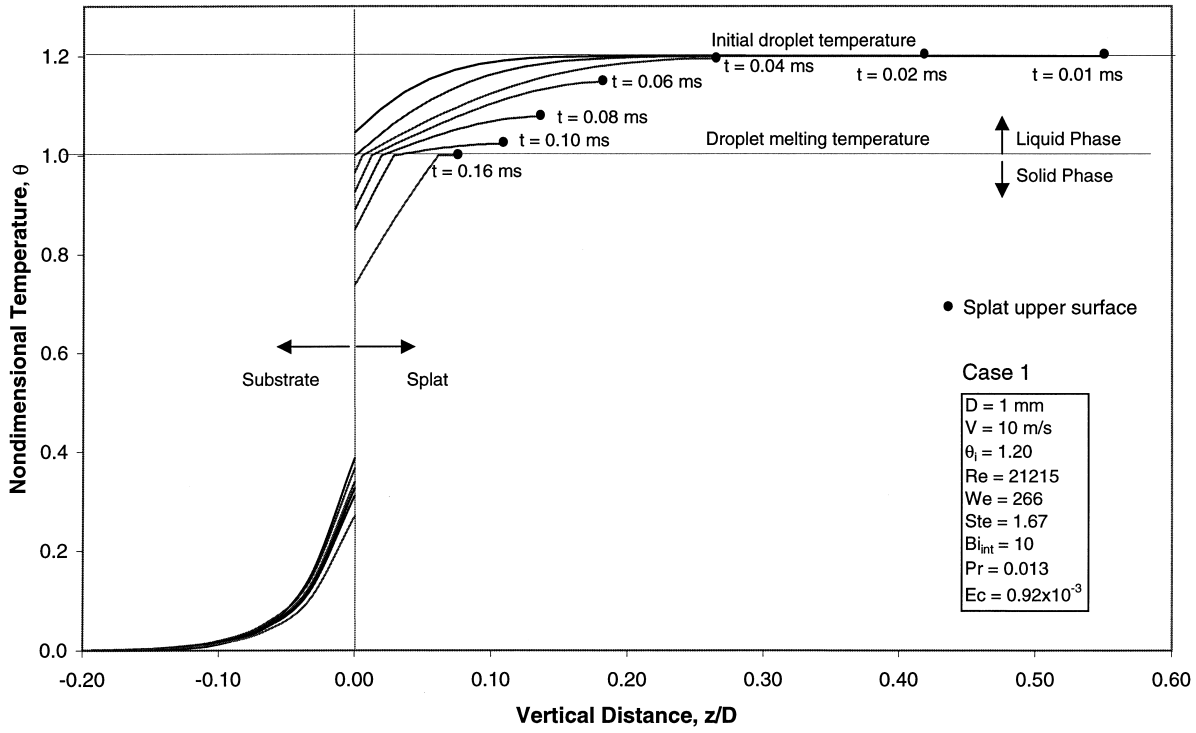

Fig. 6. Temperature evolution along the axis of the splat.

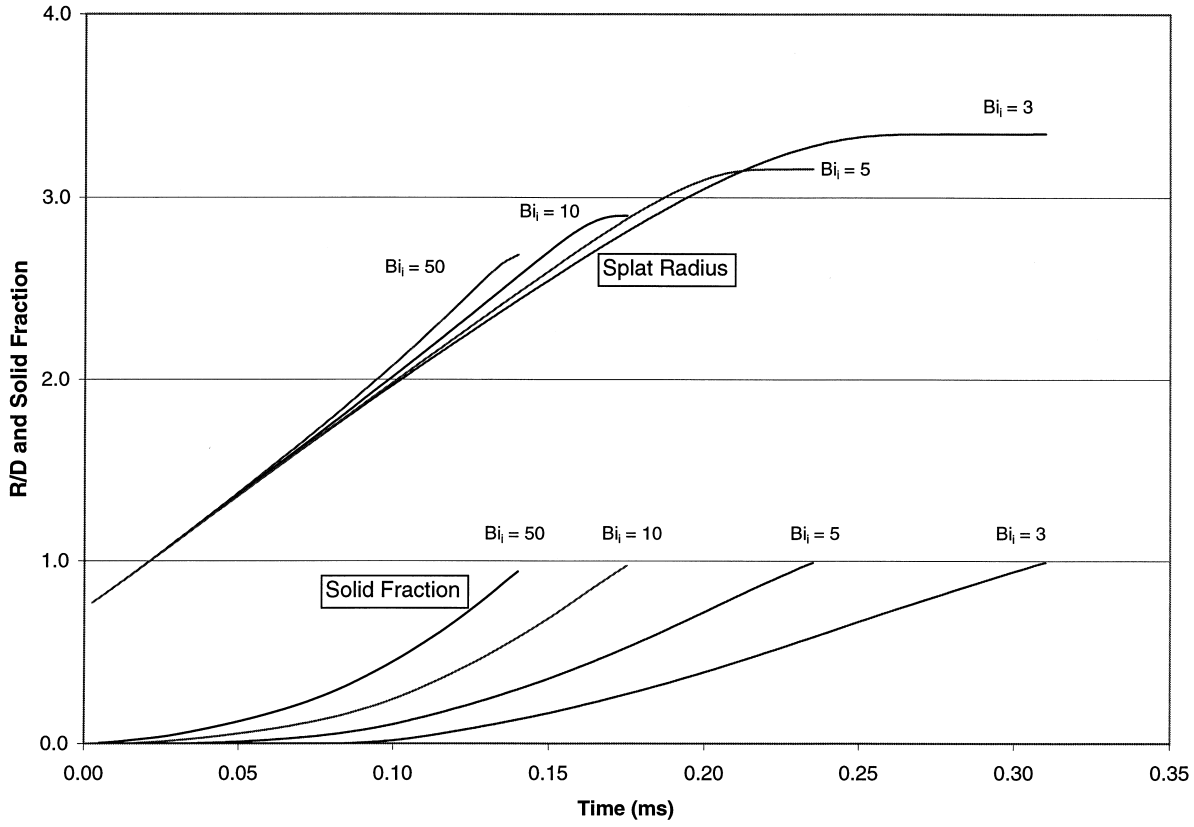

Fig. 7. Contact resistance effect on splat spreading and solidification.

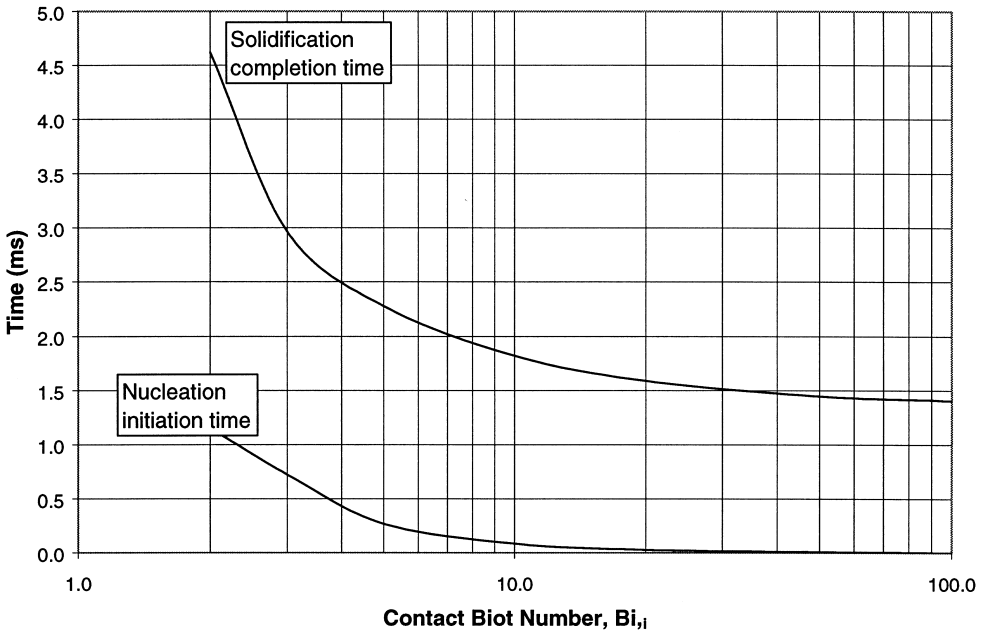

(a)

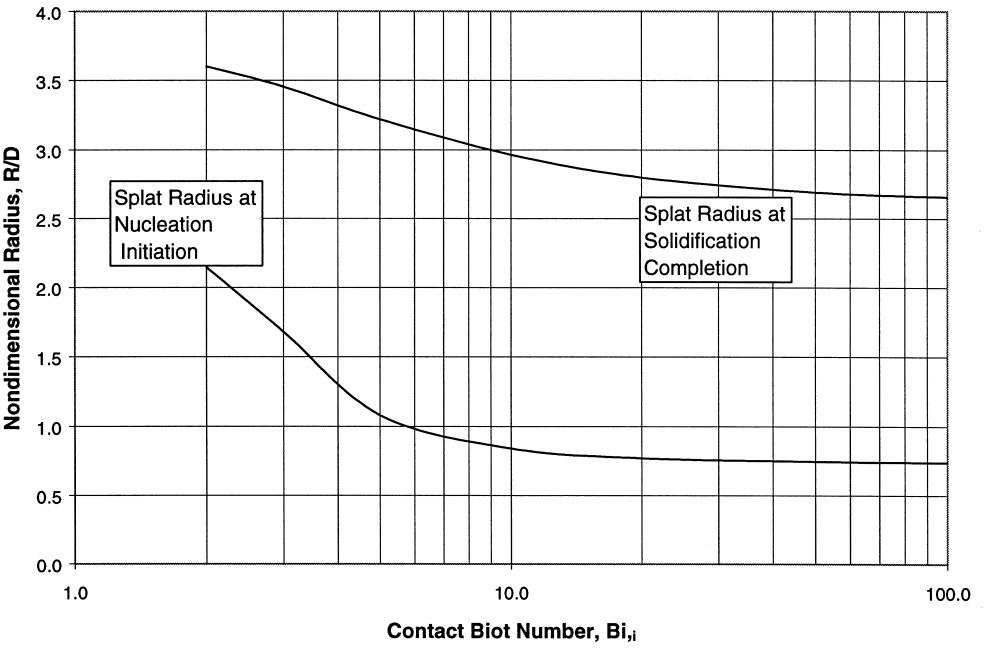

(b)

Fig. 8. Effect of contact resistance on process times and splat size.

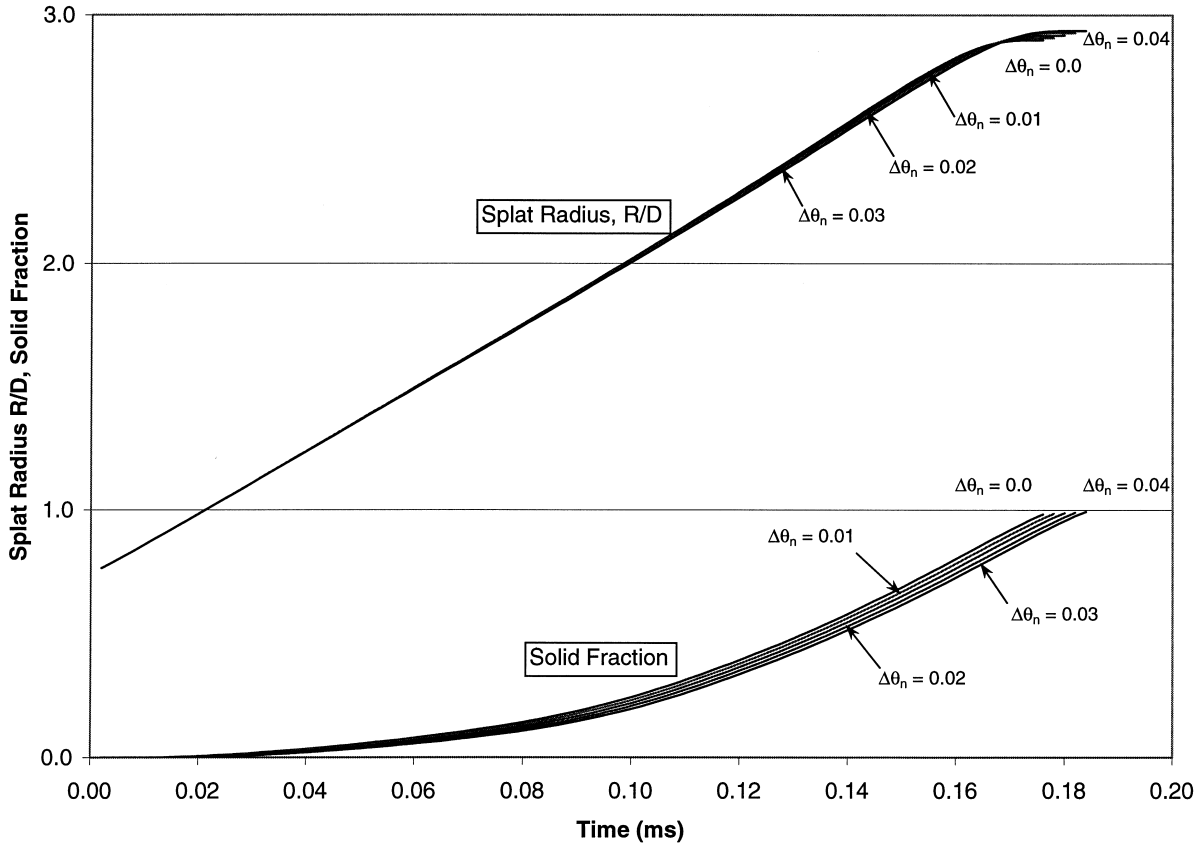

Fig. 9. Effect of nucleation temperature (undercooling) on splat spreading and solidification.

This means that thinner and wider coatings are attained with higher contact resistance.

3.3. Effect of undercooling

Nucleation delay accompanied by rapid solidification alters the heat transfer process by changing the phase change interface temperature from its thermodynamic equilibrium temperature. It is obvious from the nondimensional energy equation and boundary conditions that the magnitude of the undercooling effect depends on two key parameters namely; the magnitude of nucleation temperature relative to initial liquid superheat and the speed of solidification. Fig. 9 shows the effect of nucleation temperature on the splat radius evolution and solidification progress. The figure shows that the effect of nucleation temperature associated with undercooling is rather minor. In some cases where the liquid initial temperature is close to the melting point the undercooling effect can be more significant. Fig. 10 shows the changes in the splat radius as well as in the nucleation and complete solidification times relative to the corresponding values when undercooling is neglected. The delta-quantities are defined as

$$\Delta R = R\,(\text{with undercooling}) - R\,(\text{without undercooling}) \tag{7}$$

$$\Delta\tau = \tau\,(\text{with undercooling}) - \tau\,(\text{without undercooling}) \tag{8}$$

The subscript 'nucle' stands for the onset of nucleation while 'solid' stands for the completion of solidification. Roughly speaking, the effects of undercooling on time delay and the radius increase of nucleation and completion of solidification are linearly dependent on the degree of departure of nucleation temperature from the thermodynamic equilibrium temperature.

4. Conclusions

A numerical procedure for simulation of metal droplet deposition processes with solidification including

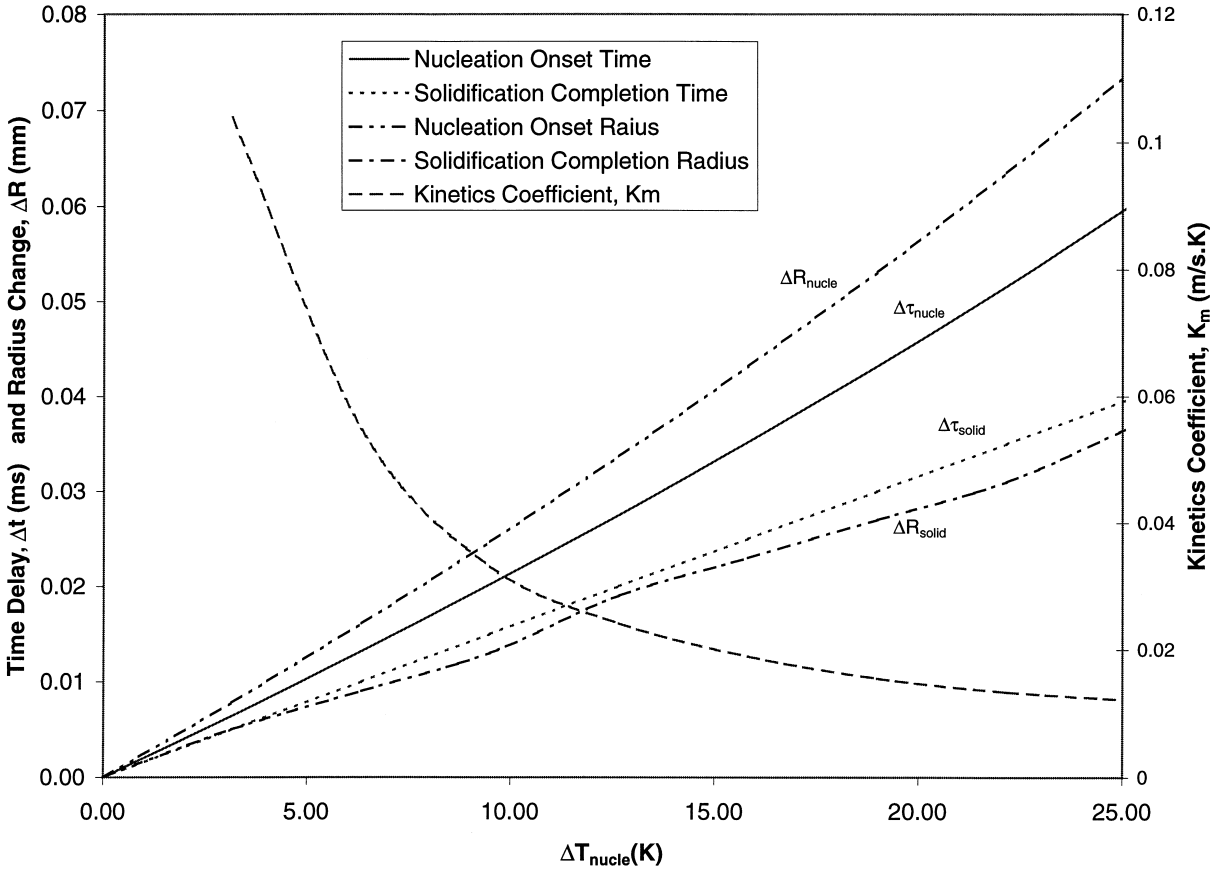

Fig. 10. Time delays and corresponding splat size variations induced by undercooling.

undercooling and contact resistance effects is utilized to study the effects of several processing parameters. The parametric study reveales that the droplet impinging velocity has strong effects on the dynamics of the liquid flow and solidification process. It also affects the final shape and size of the solidified droplet. Contact resistance also has strong effects on spreading and solidification through nucleation delay and the reduction of temperature gradient at the interface. The effects of undercooling are not significant unless the nucleation point is low in relation to the initial liquid super heat.

Acknowledgements

This study has been supported by grants from the Yeungnam University Foreign Exchange Program and Korea Science and Engineering Foundation (KOSEF) through Basic Research Grant (No. 95-0200-0402-3) while the first author was on Sabbatical at the University of California, Irvine. We also acknowledge support from the DOE/Los Alamos Laboratory through a CULAR grant and from the National Science Foundation (NSF-CTS96 14653).

References

[1] N. El-Kaddah, J. Mckelliget, J. Szekely, Heat transfer and fluid flow in plasma spraying, Metallurgical Transactions B — Process Metallurgy 15B (1984) 59–70.
[2] J. Madejski, Solidification of droplets on a cold surface, Int. J. Heat and Mass Transfer 19 (1976) 1009–1013.
[3] J.P. Delplanque, R.H. Rangel, An improved model for droplet solidification on a flat surface, Journal of Materials Science 32 (1997) 1519–1530. J.M. Hill, One-Dimensional Stefan Problems: An Introduction, Longman Scientific & Technical, 1987, pp. 12–18.
[4] A.J. Markworth, J.H. Saunders, An improved velocity field for the Madjeski splat-quenching solidification model, Int. J. Heat and Mass Transfer 35 (7) (1992) 1836–1837.
[5] H. Liu, E.J. Lavernia, R.H. Rangel, Numerical simulation of substrate impact and freezing of droplets in

plasma spray processes, Journal of Physics D: Applied Physics 26 (1993) 1900–1908.
[6] C. San Marchi, H. Liu, E.J. Lavernia, R.H. Rangel, Numerical analysis of the deformation and solidification of a single droplet impinging onto a flat substrate, Journal of Material Science 28 (1993) 3313–3321.
[7] T. Watanabe, I. Kuribayasi, T. Honda, A. Kanazawa, Deformation and solidification of a droplet on a clod substrate, Chemical Engineering Science 47 (12) (1992) 3059–3065.
[8] C.H. Amon, K.S. Schmaltz, Thermal issues in shape deposition manufacturing, in: 1996 TMS Annual Meeting, Feb. 4–8, Anaheim, CA, 1996.
[9] B. Kang, J. Waldvogel, D. Poulikakos, Remelting phenomena in the process of splat solidification, Journal of Material Science 30 (1995) 4912–4925.
[10] R.H. Rangel, X. Bian, The inviscid stagnation-flow solidification problem, Int. J. Heat and Mass Transfer 39 (8) (1996) 1591–1602.
[11] R.H. Rangel, X. Bian, Numerical solution of the inviscid stagnation-flow solidification problem, Numerical Heat Transfer — Part A 28 (November) (1995) 589–603.
[12] R.H. Rangel, X. Bian, Metal-droplet deposition model including liquid deformation and substrate remelting, Int. J. Heat and Mass Transfer 40 (11) (1997) 2549–2564.
[13] Z. Zhao, D. Poulikakos, J. Fukai, Heat transfer and fluid dynamics during the collision of a liquid droplet on a substrate — I. Modeling, Int. J. Heat and Mass Transfer 39 (1996) 2771–2789.
[14] J.P. Delplanque, E.J. Lavernia, R.H. Rangel, Multidirectional solidification model for the description of micropore formation in spray deposition process, Numerical Heat Transfer Part A — Application 30 (1996) 1–18.
[15] M. Pasandideh-Fard, R. Bhola, S. Chandra, J. Mostaghimi, Deposition of tin droplet on a steel plate: simulations and experiments, Int. J. Heat and Mass Transfer 41 (1998) 2929–2945.
[16] G.X. Wang, E.F. Matthys, Experimental investigation of interfacial conductance for molten metal drop impinging on a substrate: cooling, solidification and heat transfer coefficient, Journal of Heat Transfer 118 (1996) 157–163.
[17] G.X. Wang, E.F. Matthys, Numerical modeling of phase change and heat transfer during rapid solidification processes: use of control integrals with element subdivision, Int. J. Heat and Mass Transfer 35 (1992) 141–153.
[18] C.G. Levi, The evolution of microcrystalline structures in supercooled metal powder, Metall. Trans. A 19A (1988) 699–708.
[19] B. Kang, Z. Zhao, D. Poulikakos, Solidification of liquid metal droplets impacting sequentially on a solid surface, ASME Journal of Heat Transfer 116 (1994) 436–445.
[20] M. Chung, R.H. Rangel, Simulation of metal droplet deposition with solidification including undercooling and contact resistance effects, Numerical Heat Transfer — Part A 37 (3) (2000) 201–226.
[21] N. Özisik, in: Heat Conduction, 2nd ed., Wiley, New York, 1993, pp. 398–400.